Published in final edited form as:
Sci Transl Med. 2013 September 4; 5(201): 201ra120. doi:10.1126/scitranslmed.3005983.

Hedgehog agonist therapy corrects structural and cognitive deficits in a Down syndrome mouse model

Ishita Das[1], **Joo-Min Park**[2,3], **Jung H. Shin**[4], **Soo Kyeong Jeon**[2], **Hernan Lorenzi**[1,†], **David J. Linden**[2], **Paul F. Worley**[2], and **Roger H. Reeves**[1,*]

[1]Dept. of Physiology and Institute for Genetic Medicine, Johns Hopkins University School of Medicine, Baltimore, MD 21205

[2]Department of Neuroscience, Johns Hopkins University School of Medicine, Baltimore, MD 21205

[3]Department of Physiology, Jeju National University School of Medicine, Jeju 690-756, South Korea

[4]Institute on Alcohol Abuse and Alcoholism, NIH, Rockville, MD

Abstract

Down syndrome (DS) is among the most frequent genetic causes of intellectual disability, and ameliorating this deficit is a major goal in support of people with trisomy 21. The Ts65Dn mouse recapitulates some major brain structural and behavioral phenotypes of DS, including reduced size and cellularity of the cerebellum and learning deficits associated with the hippocampus. We show that a single treatment of newborn mice with the sonic hedgehog pathway agonist, SAG1.1 (SAG), results in normal cerebellar morphology in adults. Further, SAG treatment at birth rescued phenotypes associated with hippocampal deficits that occur in untreated adult Ts65Dn mice. This treatment resulted in behavioral improvements and normalized performance in the Morris Water Maze task for learning and memory. SAG treatment also produced physiological effects and partially rescued both NMDA receptor dependent synaptic plasticity and NMDA/AMPA receptor ratio, physiological measures associated with memory. These outcomes confirm an important role for the hedgehog pathway in cerebellar development and raise the possibility for its direct influence in hippocampal function. The positive results from this approach suggest a possible direction for therapeutic intervention to improve cognitive function for this population.

*To whom correspondence should be addressed: Biophysics 201, 725 N. Wolfe St., Baltimore, MD 21205, rreeves@jhmi.edu.
†Current address: The J. Craig Venter Institute, Rockville, MD.

Author contributions:
ID performed and analyzed anatomical data and behavioral experiments with RHR.
JMP performed hippocampal electrophysiology and analyzed the data with DJL and PFW.
JHS performed the cerebellar electrophysiology and analyzed the data with DJL and PFW.
HL performed stereology on P6 dentate gyrus and analyzed with RHR.
ID and RHR designed the overall study and wrote the manuscript.
All authors contributed to the manuscript.
RHR conceived and coordinated the project.

Competing interests:
The authors declare no competing interests. Dr. Reeves is a member of Science Advisory Boards of the Down Syndrome Research and Treatment Foundation, Research Down Syndrome, the Linda Crnic Institute and the National Down Syndrome Society; none of these positions are remunerated.

Introduction

Trisomy for human chromosome 21 (Hsa21) results in Down syndrome (DS), which is among the most complex genetic conditions compatible with survival past term (1). Mouse models with segmental trisomy for orthologs of Hsa21 genes show a number of complex outcomes with regard to development and function that are relevant to DS (2). A phenotype-based approach made possible by these animal models has supported progress in understanding many outcomes of trisomy and has led to the development of therapeutic interventions (3–6).

The cerebellum is much smaller and hypocellular in people with DS (7), and in the Ts65Dn and other mouse models (8, 9). A hallmark of the Ts65Dn cerebellum, reduced density of granule cell neuron (GC) cell bodies in the internal granule layer (IGL), also occurs in people with DS across the entire lifespan (8). A critical reason for the reduced number of cerebellar GC in trisomic adults is a substantial reduction in the rate of cell division of trisomic granule cell precursors (GCP) in the first days after birth. This reduction has been related to a prolonged cell cycle and results at least in part from the attenuated response of trisomic GCP to the mitogenic effects of Sonic hedgehog (Shh) growth factor (10, 11), the major mitogen for this cell population (12–14). When we administered a Shh pathway agonist, known as SAG, subcutaneously to trisomic Ts65Dn mice on the day of birth, we observed increased proliferation of GCPs. This treatment normalized GCP number six days later (P6) when Ts65Dn mice normally have a significant deficit in this cell population (10). Despite the initial delay, the mitotic index of GCPs in untreated trisomic mice reached the same rate as in euploid animals by postnatal day 6 (P6).

SAG 1.1 (SAG) is a derivative of chlorobenzo [*b*] thiophene, which was identified as a Shh pathway agonist (15, 16). SAG binds to and activates Smo, thus up-regulating the canonical Shh pathway and reproducing many activities of Shh in vitro. It is a small molecule that crosses the gut, the placenta and the blood brain barrier (10, 16, 17). SAG has been shown to stimulate division of neurons in the subgranular zone of the dentate gyrus after oral administration to adult mice (18). SAG has recently been given to newborn mice to stimulate GCP division, thereby counteracting the inhibition of GCP proliferation caused by administration of glucocorticoids (17).

The cognitive impairment seen in Ts65Dn, the most widely studied mouse model of Down syndrome, arises due to structural and functional differences in the trisomic brain compared to euploid (2, 8, 19–23). Several potential therapeutic approaches converge on the hippocampus because of its central role in learning and memory, functions that are disrupted in mouse models and also in people with DS (24, 25). Ts65Dn mice are markedly impaired in learning and memory, as evidenced by their performance in the Morris Water Maze, and are quite different from euploid animals in the induction of LTP in the CA1 and dentate gyrus of the hippocampus (26–28).

Here we asked whether the positive effects on cerebellar development of perinatal treatment with SAG would persist in adult trisomic mice and what this might imply as a model for therapy in DS.

Results

SAG treatment at birth normalizes cerebellar structure in adult mice

We synthesized SAG as described (15) and compared its ability to stimulate proliferation of GCP relative to dually lipidated sonic hedgehog (Shh-Np) (Fig. S1). Newborn pups were injected with 20 μg/g of SAG. This dose successfully normalizes proliferation of GCP in Ts65Dn mice for the first week of life, stimulates the Shh pathway in utero when given orally to pregnant dams, and stimulates proliferation of cells in the dentate gyrus in young adult mice (10, 16, 18). A dose in the same range (14.0 – 25.2 μg/kg) induces maximum expression of a Gli-luciferase reporter of Shh pathway activity in the brain (17).

At about 16 weeks of age we determined cerebellar area at the midline in sagittal sections and cerebellar GC density of SAG-injected Ts65Dn mice (TsSAG), euploid animals injected with vehicle (EuVeh), and vehicle-injected trisomic animals (TsVeh) (Fig. 1). Adult TsSAG mice that received a single injection of SAG on the day of birth had the same cross-sectional area and GC density as EuVeh, and both were significantly greater than TsVeh (Fig. 1a–c and Table S1). We showed previously that a single dose of SAG given to euploid mice (EuSAG) at P0 did not significantly increase GCP number at P6 (10).

We and others have shown that the number of granule cells in DG is reduced in Ts65Dn mice as early as P6, an effect that persists through the first year of life and presumably beyond (20, 21). Adult DG cell number is also influenced by external factors, such as activity or nutrition (29, 30). Accordingly, we looked for acute SAG effects on proliferation in the DG by co-injecting BrdU and SAG at P0 and analyzing cell number at P6. In contrast to the normalization of cerebellar granule cell number six days after injection of SAG (10), the DG deficit in Ts65Dn mice that received SAG treatment was not ameliorated (Fig. 1d). TsVeh and TsSAG mice were not different from each other, and both showed a lower rate of proliferation in DG after SAG and BrdU labeling than did EuVeh (Fig. 1d and S2; Tables S2 and S3).

SAG does not normalize Long Term Depression (LTD) from cerebellar Purkinje cells

We asked whether normalization of cerebellar morphology would affect the synaptic function of cerebellar circuits measured in brain slice preparations. Excitatory postsynaptic currents (EPSCs) were recorded from Purkinje cells in lobule III and in lobule IX (Fig. 2), because there are known differences in electrophysiological properties between these areas (31). Despite the pronounced morphological differences between the Ts65Dn and euploid cerebellum, we did not find differences in EPSC kinetics as indexed by rise time or decay tau in either lobule III or lobule IX (Table S4).

As an index of release probability at presynaptic terminal of GCs, we measured EPSC paired-pulse ratios (PPRs). PPRs were significantly lower in trisomic mice than in euploid in both lobule III and lobule IX ($p=0.0009$ and 0.0006, respectively) (Fig. 2b and Table S4).

SAG treatment did not restore the PPR values in trisomic mice. The lower PPR values in Ts65Dn suggest that release probability is increased at these synapses. This is consistent with a recent report that cerebellar GCs (the cells of origin of the parallel fiber axons) in Ts65Dn mice show increased excitability and larger action potential amplitude (32). We did not find any significant differences in LTD expression in either lobule III or lobule IX (Table S4). SAG treatment of Ts65Dn mice resulted in more depression of EPSC after the induction of LTD (p=0.019), but this was limited to lobule III. Accordingly, it is difficult to relate therapeutic actions of SAG to effects on LTD. SAG treatment of Euploid mice significantly decreased the PPR values measured in lobule IX (p=0.005), but did not affect any other parameters.

SAG normalizes performance in hippocampal but not prefrontal tasks

Ts65Dn mice have been tested in numerous open field paradigms for hyperactivity and anxiety levels, with highly inconsistent results (Reviewed in (*2*)). We used the open field to look for gross effects on general locomotor function while familiarizing the mice to handling. These procedures were not powered to detect small differences consistent with anxiolytic or anxiogenic effects (power is 60%). We found that the time spent in the periphery or center of the maze was similar for EuVeh and TsVeh groups, and no significant differences were observed with TsSAG (Fig. S3). Separate measurements were made for the number of rearings and the number of beam breaks at the center or at the periphery, and these were further categorized into fine motor activity or ambulatory activity if the same beam was broken twice or if consecutive beams were broken, respectively (Fig. S3 and Table S5).

Next we assessed a previously described deficit of Ts65Dn in the Y maze test of working memory, a non-aversive task that does not involve training or a strong stimulus (see reference (2)). EuVeh mice (n=13) showed an average of 78% alternation. TsSAG and TsVeh mice were significantly impaired, with both groups showing only ~60% alternation (EuVeh vs. TsSAG, p = 0.003; EuVeh vs. TsVeh p = 0.0001, Fisher's LSD) (Fig. S4a and Table S6). With more power to detect differences in activity than in open field (est. 85%), we observed significantly more activity, measured as number of arm entrances, in trisomic mice with or without SAG than in euploid mice (EuVeh vs. TsSAG, p = 0.001; EuVeh vs. TsVeh, p = 0.002, Fisher's LSD) (Fig. S4b). SAG treatment did not have an effect on either outcome in Ts65Dn mice, nor did it alter outcomes in EuSAG compared to EuVeh.

Multiple investigators have reported that Ts65Dn mice display a robust deficit in hidden platform and probe component of the Morris Water Maze task (MWM)(summarized in (*2*)). All four groups of mice tested here performed similarly in the visible platform component, as expected (Fig. 3a and Table S7). Swimming velocities were not different between groups (Fig. S5a). In the hidden platform paradigm, mice learn to navigate to the platform using visuospatial cues outside the tank. As expected, TsVeh mice had prolonged escape latencies compared to EuVeh. Bonferroni-corrected p values showed a significant difference between TsVeh and EuVeh in pairwise comparison (corrected p value =0.003). The pairwise comparisons were preceded by two way repeat measure (RM) ANOVA, which indicated a significant difference between the three groups, ($F(2,29) = 6.5$, $p = 0.005$, $\alpha = 0.05$). TsSAG

mice had similar escape latencies as EuVeh mice (p = 0.91) and latencies for both groups were significantly shorter than latencies for TsVeh mice (TsSAG vs. TsVeh, corrected p value = 0.042 (Fig. 3b and Table S8). The improvement in learning was also evident in the probe test (Fig. 3c and 3d and Table S9) (Kruskal Wallis rank test, p = 0.001; using Mann Whitney test for pair-wise comparison, for TsVeh vs. TsSAG and TsVeh vs. EuVeh, p = 0.001 and 0.0001, respectively) and reflected improved strategies for platform finding in TsSAG mice compared to TsVeh (Fig. S5). SAG treatment had no effect on the performance of euploid mice (Fig. 3).

We evaluated the strategy used to find the platform based on an analysis of trajectory and latency as described (33) (Supplementary notes regarding behavior studies; Fig. S5b and c; Table S10). These parameters provide a detailed picture of spatial learning in the MWM that is not obtained from distance travelled alone. TsSAG mice used the same successful strategies as EuVeh, while the greatly increased latency for TsVeh mice was correlated with inefficient strategies. The strategy scores were highly correlated with latency in all three groups (Spearman's rho >0.80) indicating that time taken to find the platform was strongly related to the strategy.

Hippocampal physiology is partially normalized by SAG treatment

To determine whether improvements in MWM reflect physiological changes in the hippocampus, we employed two different measures to characterize basal synaptic transmission. The first was to derive an index of synaptic strength by varying stimulus strength, thereby constructing an input-output plot relating presynaptic fiber volley (FV) amplitude to the onset slope of the field excitatory postsynaptic potential (fEPSP) (Fig. 4a and Table S11). Second, we estimated the probability of neurotransmitter release by application of pulse pairs delivered at intervals ranging from 30 to 150 msec. The paired-pulse ratio serves as an index of release probability in this synapse (Fig. 4b and Table S12). Both of these measures revealed similar basal synaptic properties in EuVeh, TsVeh and TsSAG mice.

LTP evoked by theta burst stimulation (TBS) results in a rapid and sustained increase of AMPAR-mediated responses in Schaffer collateral-CA1 synapses (34). In hippocampal slices derived from EuVeh mice, fEPSP was increased to 138.6±3.4 % (n=12) of baseline at t=30 min after stimulation and sustained at the level of 127.3±3.7 % of baseline at t=80 min. (Fig. 4c and Table S13). TBS-induced LTP in TsVeh was significantly reduced (123.6±2.3 % of baseline at t= 30 min, p=0.001) and continued to decay more rapidly than euploid control mice (117.4±2.7 % of baseline at t=80 min, p= 0.038), consistent with previous findings (34). However, in acute hippocampal slices derived from TsSAG mice, the magnitude of TBS-induced LTP was significantly increased compared to TsVeh (132.9±2.2 % of baseline at t=30 min, p=0.006) and not different from euploid (127.4±2.0 % of baseline at t=80 min., p=0.97).

We examined synaptic properties that might underlie reduced LTP in Ts65Dn. The current-voltage relationship of evoked EPSCs in Schaffer collateral-CA1 synapses was similarly linear in euploid and Ts65Dn mice (Fig. 5a and Table S14), indicating no difference in calcium-permeable AMPARs. Next, we monitored the amplitude of evoked EPSCs using

conditions that separately reveal AMPA receptor- and NMDAR-dependent responses. The ratio of the NMDA/AMPA receptor-dependent responses in Ts65Dn mice was dramatically reduced compared to the euploid mice (Fig. 5b and Table S15) (p= 0.06 ± 0.011 in Ts65Dn, n=11; 0.39 ± 0.059, n=13 in euploid; p=0.00002) The NMDA/AMPA ratio in TsSAG (0.19 ± 0.034, n=11) was significantly increased compared to TsVeh mice (p=0.003) but was not restored to euploid levels p=0.006). This is consistent with the reduction of NMDAR-dependent LTP in Ts65Dn mice and enhancement of NMDAR-dependent LTP in SAG-treated animals.

Discussion

Granule cell precursors in cerebellum of newborn Ts65Dn mice demonstrate a short lag in the initiation of the burst of proliferation relative to euploid (10). Acute SAG treatment stimulates the division of trisomic cells, and here, a single treatment on the day of birth was sufficient to overcome the transient proliferation deficit and normalize cerebellar structure in adult Ts65Dn mice. Ts65Dn mice do not show behavioral measures of cerebellar dysfunction in typical assays such as the accelerating Rota-Rod(8, 35). Accordingly, our analysis focused on electrophysiological measures and revealed that SAG treatment is linked to a modest increase of LTD in lobule III (but not lobule IX) of Ts65Dn. In contrast, a single treatment with SAG resulted in robust improvement in learning and memory behavior in assays that are sensitive to hippocampal function, and to improved NMDA receptor function and synaptic plasticity. The persistence of these improvements is striking, and invites comparison with reports of persistent improvements of cognition and LTP after pharmacological treatment of adolescent Ts65Dn mice with GABA-A antagonists (36, 37). Understanding the basis for these long-term therapeutic effects may have implications for treating DS, and the current results should encourage further exploration of a possible role for Shh in perinatal programming of hippocampus.

SAG penetrates the blood brain barrier (10, 16, 18) and can be anticipated to activate Shh signaling in cerebellar and hippocampal neurons. We did not see compensation of the small deficit in the number of replicating cells in dentate gyrus of Ts65Dn by perinatal SAG treatment. From this result it appears that normalization of DG cell number is not a necessary condition for normalizing the several behavioral and physiological outcomes in Ts65Dn mice that were assessed in this study. Normalization of cerebellar morphology might contribute to improved behavioral outcomes in the MWM. The cerebellum plays an important role in spatial learning, where it is involved in the acquisition of optimal strategies in tasks in which memory is a component, including the MWM hidden platform (33, 38–42). Here, improved learning and memory were correlated with normalization of cerebellar morphology after SAG treatment. These results are consistent with a role of cerebellum in spatial learning, and suggest that the marked cerebellar hypoplasia in DS may contribute to some cognitive deficits, as well.

Up-regulation of the Shh pathway by SAG has now been shown to be efficacious in several situations. In addition to correction of cerebellar hypoplasia in trisomic models, Shh or SAG can support proliferation of neural precursors *in vivo* after spinal cord injury in rats (43). SAG administration can also counter the anti-proliferative effects of glucocorticoids on

cerebellar GCPs in newborn mice (17, 43). A number of ciliopathies have pathology related to disruption of hedgehog signaling (44) and SAG might have a therapeutic role in ameliorating some of these effects.

However, pharmacological stimulation of the Shh pathway in newborn infants as a therapeutic strategy might be problematic. Hedgehog signaling plays a central role in many fundamental aspects of development including axis formation and generation of neural crest, and many of its effects are dosage sensitive. Shh is also required for stem cell generation and maintenance in differentiated tissues. Chronic Shh pathway stimulation is observed in a number of tumor types and directly linked to an increased incidence of medulloblastoma (45, 46). SAG-treated mice studied here showed no evidence of tumor formation or obvious complications in the first four months of life. Before a clinical application is contemplated in people with DS, however, it will be necessary to better understand the SAG role in hippocampal function and the sensitivity to possible side-effects on different genetic backgrounds, while refining both the dosage and the route of drug administration. It would be useful to understand why trisomic GCP (and possibly other trisomic cells) have an attenuated response to the mitogenic effects of Shh, which might offer further targets for therapy (47). We note that there is no evidence in our data and no current theoretical basis for a positive role of Shh pathway stimulation at birth on cognitive ability in euploid adults.

We demonstrated the efficacy of a possible approach to the improvement of learning and memory in a trisomic mouse model. A single injection of a Shh pathway agonist on the day of birth corrected a key developmental deficiency in cerebellum, restoring normal structure in adults. This single treatment evoked a positive and lasting effect on hippocampal-dependent learning and memory, and partially normalized hippocampal synaptic NMDA receptor function and NMDAR-dependent LTP expression. These observations suggest a possible approach to ameliorate cognitive deficits that occur as a consequence of trisomy 21.

Materials and Methods

Study design

Our previously published studies show that the Ts65Dn mouse displays and predicts aspects of cerebellar pathology that occur in people with DS, that the cerebellar hypoplasia is substantially due to an attenuated response of gcp to the mitogenic effects of Shh growth factor in the period close to the time of birth and that stimulation of the Shh pathway with systemic application of SAG at P0 eliminates the gcp deficit at P6 (8, 10). Based on these findings, we designed a study to determine whether these salutary effects of SAG might extend beyond the perinatal period. We injected animals at birth with a dose of SAG that produced salutary effects in previous studies from our lab and others (10, 16–18). One set of animals was prepared for behavior studies based on our prior determination of variation/cohort size required to power a significant analysis of the MWM paradigm, which is robustly affected in Ts65Dn mice. Similarly, sample sizes for the cohorts subjected to the standard electrophysiological paradigms tested here were chosen based on prior experience. Statistical analyses are described in detail below. In all cases, investigators performing tests were blind to genotype and treatment.

Animals

Founder B6EiC3H-*a/A*-Ts65Dn (Ts65Dn) mice were obtained from the Jackson Laboratory and maintained in our colony as an advanced intercross on a (C57BL/6J x C3H/HeJ) background.

SAG was synthesized as described (15), dissolved in ethanol or DMSO and resuspended in triolein. Activity of this batch of SAG was established by comparison to the amount of GCP proliferation relative to Shh (10, 15) (Fig. S1). Each pup in a given litter received a subcutaneous dose of 20 μg/g of SAG or vehicle in 20 μl.

Behavior testing—Animals were given a coded i.d. by someone other than the investigator so that all tests were performed by investigators who were blind to genotype and treatment group. Tests were performed in the following order: open field, Y maze, MWM. The open field test was conducted in the Photobeam activity system (San Diego Instruments) in a novel room to which the mice had not been habituated prior to the test. Mice were placed in a clear acrylic container (16″ (W) x 16″ (D) x 15″ (H)) for 90 min in the first phase and 50 minutes in the second phase. The numbers of movements at the center, movements at the periphery and rearings were recorded. Normalized activity is defined as the number of beam breaks at the center or periphery divided by the total number of beam breaks by the mouse. This was further categorized as fine motor activity (if the same beam is broken twice sequentially) or ambulatory activity (if contiguous beams are broken). Data shown are from both phases of open field testing (Table S5).

For the Y maze, mice were habituated to handling for 3 days. They were released on a randomly chosen arm of a stainless steel Y shaped apparatus and movements were tracked for 5 minutes using the SMART program (San Diego Instruments). An entrance was scored when the head and front two paws were in an arm > 0.2 s (Table S6).

Morris water maze (MWM) was initiated a week after Y maze (9). A tank of 120 cm diameter was filled with dilute latex paint at 19°–22° C. For the visible platform test, the position of a platform submerged about 1 cm below the surface was indicated with a flag. This test was conducted on 1 day with 3 blocks of trials of four attempts each lasting up to 60 s. The position of the cued platform was changed for each attempt in each trial (Table S7). The hidden platform test was conducted ten days later with the platform always in the same position for three training days. Latency and path were recorded (Table S8). The following day, the platform was removed for the Probe Trial, when mice were allowed to swim for 3 min and the time spent in each quadrant was measured (Table S9). Tracks followed by the mice were extracted using the SMART program (San Diego Instruments) and scored using a modification of the method of Petrosini et al. (38) (Fig. S4, Table S10).

Histological measurements—Tissue harvest and histological preparation were performed as described (8). Relative midline sagittal area of the cerebellum was measured using Image J and normalized to the midline area of the entire brain. Unbiased stereology was performed with Stereologer 1.3 (SPA Inc.) on 30 μm sections of the brain of P6 animals. The Optical disector [sic] method was used to obtain density and Cavalieri's principle was used to estimate volume (48). The frame area of the disectors was 169 μm^2,

depth of 10 μm and guard height of 5 μm. Disectors were spaced at intervals of 95 μm. Nuclei were counted at 500X. The coefficient of error within and between samples was ≤ 10%. The sampling fraction was 1 in 6 sections. On average 13 sections per animal were sampled.

BrdU at 250 mg/g was included in the SAG or vehicle preparations injected at P0. Treated mice were sacrificed at P6. The brain was fixed in 4% PFA for 14 hours at 4°C, then transferred to 20% sucrose solution with one change after 24 hours. Serial coronal sections (50 μm) that contained the hippocampus were cut from lateral 1.94 mm to −4.04 mm bregma, cf. the Mouse Brain in Stereotaxic Coordinates (46). One in 5 sections was processed for BrdU and NeuN-double labeling according to the indirect immunofluorescence method of Coons (47) with the primary mouse anti NeuN- biotin (Chemicon) and rat anti- BrdU(Novus) antibodies, followed by secondary Alexa Flour 488 donkey anti-rat IgG (Molecular Probe) and Alexa fluor 594 streptavidin (Molecular Probe) antibodies. The number of BrdU-labeled nuclei in the dentate gyrus was estimated using the principles of unbiased stereology as described above. Volume (Vref) of the chosen half of the dentate gyrus was estimated using the total area of the sampled sections (Aref), the average thickness of the sections (t) and the sampling fraction. Each sampled section was imaged using two photon excitation by the Chameleon Vision II laser (Coherent Inc.) attached to a Zeiss axioscope 710NLO microscope (Zeiss). A low magnification image was used to determine the section area. A pilot experiment determined the area and density of the optical disector placement so as to allow counting of about 15–20 nuclei per section or 100–150 nuclei per animal. On average 8 sections were analyzed per animal. An area of 21 μm × 21 μm was found to be acceptable with one disector placed every 0.02 mm^2 through the dentate gyrus. An estimate of the total number of BrdU-labeled nuclei was attained by multiplying the Vref by Nv (observed density) (Table S2 and S3).

Electrophysiology

Electrophysiology: Cerebellum—Parasagittal slices (250 μm) were obtained from EuVeh (n = 9), EuSAG (n = 5), TsVeh (n = 9), or TsSAG (n = 9) mice aged 21–28 days using a Leica vibratome in an ice-cold cutting solution containing (in mM): 225 sucrose, 119 NaCl, 2.5 KCl, 0.1 $CaCl_2$, 4.9 $MgCl_2$, 26.2 $NaHCO_3$, 1 NaH_2PO_4, 1.25 glucose, and 3 kynurenic acid bubbled with 95% O_2 and 5% CO_2. Whole-cell recordings were made from Purkinje cells in either lobule III or IX at −70 mV in aCSF containing (in mM): 124 NaCl, 2.5 KCl, 2.5 $CaCl_2$, 1.3 $MgCl_2$, 26.2 $NaHCO_3$, 1 NaH_2PO_4, 20 glucose bubbled with 95% O_2 and 5% CO_2 at room temperature. 5 μM GABAzine (Sigma) was added to block GABA-A Receptor currents. Recording electrodes contained a solution composed of (in mM): 120 Cs-methanesulfonate, 10 CsCl, 10 HEPES, 0.2 EGTA, 4 Na_2-ATP, 0.4 Na-GTP (pH = 7.25). Paired stimulations (50 ms apart) were done with a glass electrode filled with aCSF by passing 20–40 μA of current with 0.2 ms duration to evoke EPSCs having around 200 pA amplitude. LTD was induced by a train of 10 stimuli at 100 Hz depolarizing the postsynaptic cells to 0 mV, which was repeated 30 times every 2 s. Currents were filtered at 1 kHz and measured with Multiclamp 700B (Molecular Devices), and acquired with Clampex software (Molecular Devices) at 5 kHz. EPSC amplitudes, rise-time, and decay tau were measured

off-line using Clampfit software (Molecular Devices). Two-way ANOVA was used for statistical analysis (Table S4).

Electrophysiology: Hippocampus

Slice Preparation—Transverse hippocampal slices (400 μm thick) were prepared at P90-120 by cutting on a tissue slicer in ice-cold dissection buffer (in mM): 110 choline chloride, 2.5 KCl, 7 $MgCl_2$, 0.5 $CaCl_2$, 2.4 sodium pyruvate, 1.3 sodium L-ascorbate, 1.2 NaH_2PO_4, 25 $NaHCO_3$, and 20 D-glucose. Slices were recovered for 3–6 hr at room temperature in artificial cerebrospinal fluid (aCSF) composed of (in mM): 124 NaCl, 2.5 KCl, 1.3 $MgCl_2$, 2.5 $CaCl_2$, 1 NaH_2PO_4, 26.2 $NaHCO_3$, and 20 D-glucose) and saturated with 95 % O_2, 5 % CO_2. Hemislices were recorded in an interface chamber, maintained at 32 °C for 1 hr, and perfused continuously with aCSF at a rate of 3 ml/min.

Field potential recording—fEPSPs were recorded from the stratum radiatum of acute hippocampal slices in response to stimulation of the Schaffer collateral-commissural pathway, as described (49). Stimulus intensity was adjusted to elicit 50–60 % of the maximal fEPSP slope response. LTP was measured in Schaffer collateral-CA1 synapses. Experimenters were blind to the genotype/treatment throughout the experiments. LTP was induced by theta burst stimulation (TBS, 5 trains of 4 pulses; at 100 Hz and 200 ms apart). Evoked responses were stored on-line and analyzed off-line using Clampfit (Ver9.2). Time course of LTP was expressed as percentage of the fEPSP slope during the baseline recording (Table S11, S12, S13).

NMDA/AMPA receptor ratio and I–V curves of AMPA-evoked EPSCs—Evoked EPSCs and the peak amplitude were recorded at a holding potential of Vh =−70 mV to access AMPAR-mediated responses. NMDAR-mediated responses were nest recorded at Vh = +40 mV in the presence of the selective AMPAR antagonist 2,3-dihyroxy-6-nitro-7sulfamoyl-benzo(f)quinoxaline-2,3-dione (NBQX, 10 mM, Tocris). For I–V curves, spermine (100 μM, Sigma) was added to the pipette solution to block GluR2-lacking AMPARs at positive potentials. Evoked AMPAR-mediated responses were recorded from different membrane potentials ranging from −80 mV to +40 mV in 20 mV steps. Amplitudes of currents were normalized to the value measured at −40 mV. Whole-cell voltage-clamp recordings of hippocampal CA1 pyramidal neurons were performed in the presence of GABA-A receptor antagonist (10 mM GABAzine, Sigma) and NMDA receptor antagonist (50 mM D-AP5, Sigma). The pipette solution contained (in mM): 90 Cs-methanesulfonate, 48.5 CsCl, 5 EGTA, 2 $MgCl_2$, 2 Na-ATP, 0.4 Na-GTP, 1 QX 314 bromide, and 5 HEPES (pH 7.2, 290 ±5 mmol/kg). Statistical comparison was performed by the independent t test and ANOVA for multiple comparisons (Table S14, S15).

Statistical analysis

All statistical tests were conducted in SPSS or Sigmastat. All analyses presented here were performed specifically to compare TsVeh, TsSAG and EuVeh. In all instances where EuSAG data are reported, they are always compared to the EuVeh group in a pairwise analysis using Fisher's Least Significant Difference (LSD). All behavioral tests were

performed while the experimenter was blinded to genotype and treatment. Statistical analyses were similarly conducted blinded to genotype and treatment.

All morphological data (cell number, density and areas) were tested for normality by quantile-quantile plots or Kolmogorov- Smirnov test. Multivariate ANOVA (MANOVA, Wilk's Lambda) was carried out for cerebellar GC density and normalized area, followed by pairwise comparisons using Fisher's LSD. For GC number in the P6 dentate gyrus, pairwise comparisons between the three groups were carried out using Fisher's LSD. Normalized numbers of BrdU labeled cells in the GC were analyzed using one way ANOVA followed by Fisher's LSD. Open field data were tested using MANOVA for normalized number of fine motor and ambulatory movements at the center vs. the periphery and for the number of rearings and for spontaneous alternation and number of arm entries in the Y-maze. The value of Wilk's Lambda was determined, followed by correction for multiple pairwise comparisons using the Bonferroni method. All MWM data was tested for normal distribution using Kolmogorov- Smirnov test or quantile- quantile plots. The hidden platform data was transformed before being tested in parametric tests. The probe test data and strategy scores were analyzed using non- parametric tests. Latency to platform in the MWM was analyzed using two way repeated measures ANOVA, with the trials in visible or hidden platform included as the repeated measurement, followed by multiple pairwise comparisons between the three groups. P values were corrected by the Bonferroni method to maintain the family wise alpha value at 0.05.

Probe test results in MWM were analyzed using the non-parametric version of one way ANOVA – Kruskal Wallis Rank test, followed by Mann Whitney test for pairwise comparisons. Correlation between scores on trajectory and latency was determined using the non parametric Spearman's rho. The frequency of different scores was compared using the chi square test and Fisher's exact p value.

Supplementary Material

Refer to Web version on PubMed Central for supplementary material.

Acknowledgments

We thank Dr. David J. Meyers (JHU SOM Synthetic Core Facility) for the synthesis of SAG 1.1, which was supported in part by a grant from the Flight Attendant Medical Research Institute.

Funding:

This work was supported by the Down Syndrome Research and Treatment Foundation, Research Down Syndrome and R01 HD38384 from the National Institute of Child Health and Human Development (RHR); the intramural programs of National Institute on Alcohol Abuse and Alcoholism at the National Institutes of Health (JHS); MH51106 from the National Institute of Mental Health (DJL); and R01 NS39156 from the National Institute of Neurological Diseases and Stroke (PFW). The information presented does not necessarily reflect the opinions of the funding agencies.

References and notes

1. Antonarakis SE, Lyle R, Dermitzakis ET, Reymond A, Deutsch S. Chromosome 21 and down syndrome: from genomics to pathophysiology. Nat Rev Genet. Oct.2004 5:725. [PubMed: 15510164]

2. Das I, Reeves RH. The use of mouse models to understand and improve cognitive deficits in Down syndrome. Dis Model Mech. Sep-Oct;2011 4:596. [PubMed: 21816951]
3. Braudeau J, et al. Specific targeting of the GABA-A receptor {alpha}5 subtype by a selective inverse agonist restores cognitive deficits in Down syndrome mice. J Psychopharmacol. Aug.2011 25:1030. [PubMed: 21693554]
4. Martinez-Cue C, et al. Reducing GABAA alpha5 receptor-mediated inhibition rescues functional and neuromorphological deficits in a mouse model of down syndrome. J Neurosci. Feb 27.2013 33:3953. [PubMed: 23447605]
5. Reeves RH, Garner CC. A year of unprecedented progress in Down syndrome basic research. Ment Retard Dev Disabil Res Rev. 2007; 13:215. [PubMed: 17910083]
6. Ruparelia A, Pearn ML, Mobley WC. Cognitive and pharmacological insights from the Ts65Dn mouse model of Down syndrome. Curr Opin Neurobiol. May 30.2012
7. Crome R, Cowie V, Slater E. A statistical note on cerebellar and brain-stem weight in Down Syndrome. Journal of Mental Defect Research. 1966; 10:69.
8. Baxter LL, Moran TH, Richtsmeier JT, Troncoso J, Reeves RH. Discovery and genetic localization of Down syndrome cerebellar phenotypes using the Ts65Dn mouse. Hum Mol Genet. Jan 22.2000 9:195. [PubMed: 10607830]
9. Olson LE, et al. Down syndrome mouse models Ts65Dn, Ts1Cje, and Ms1Cje/Ts65Dn exhibit variable severity of cerebellar phenotypes. Dev Dyn. Jul.2004 230:581. [PubMed: 15188443]
10. Roper RJ, et al. Defective cerebellar response to mitogenic Hedgehog signaling in Down syndrome mice. Proc Natl Acad Sci U S A. 103:1452. ePub Jan 23, 2006. [PubMed: 16432181]
11. Trazzi S, et al. APP-dependent up-regulation of Ptch1 underlies proliferation impairment of neural precursors in Down syndrome. Hum Mol Genet. Apr 15.2011 20:1560. [PubMed: 21266456]
12. Wallace VA. Purkinje-cell-derived Sonic hedgehog regulates granule neuron precursor cell proliferation in the developing mouse cerebellum. Curr Biol. 1999; 9:445. [PubMed: 10226030]
13. Dahmane N, Ruiz-i-Altaba A. Sonic hedgehog regulates the growth and patterning of the cerebellum. Development. 1999; 126:3089. [PubMed: 10375501]
14. Wechsler-Reya RJ, Scott MP. Control of neuronal precursor proliferation in the cerebellum by Sonic Hedgehog. Neuron. 1999; 22:103. [PubMed: 10027293]
15. Chen JK, Taipale J, Young KE, Maiti T, Beachy PA. Small molecule modulation of Smoothened activity. Proc Natl Acad Sci U S A. Oct 29.2002 99:14071. [PubMed: 12391318]
16. Frank-Kamenetsky M, et al. Small-molecule modulators of Hedgehog signaling: identification and characterization of Smoothened agonists and antagonists. J Biol. Nov 6.2002 1:10. [PubMed: 12437772]
17. Heine VM, et al. A small-molecule smoothened agonist prevents glucocorticoid-induced neonatal cerebellar injury. Sci Transl Med. Oct 19.2011 3:105ra104.
18. Machold R, et al. Sonic hedgehog is required for progenitor cell maintenance in telencephalic stem cell niches. Neuron. Sep 11.2003 39:937. [PubMed: 12971894]
19. Salehi A, et al. Increased App expression in a mouse model of Down's syndrome disrupts NGF transport and causes cholinergic neuron degeneration. Neuron. Jul 6.2006 51:29. [PubMed: 16815330]
20. Insausti AM, et al. Hippocampal volume and neuronal number in Ts65Dn mice: a murine model of Down syndrome. Neurosci Lett. Sep 11.1998 253:175. [PubMed: 9792239]
21. Lorenzi HA, Reeves RH. Hippocampal hypocellularity in the Ts65Dn mouse originates early in development. Brain Res. Aug 9.2006 1104:153. [PubMed: 16828061]
22. Chakrabarti L, Galdzicki Z, Haydar TF. Defects in embryonic neurogenesis and initial synapse formation in the forebrain of the Ts65Dn mouse model of Down syndrome. J Neurosci. Oct 24.2007 27:11483. [PubMed: 17959791]
23. Belichenko PV, et al. Synaptic structural abnormalities in the Ts65Dn mouse model of Down Syndrome. J Comp Neurol. Dec 13.2004 480:281. [PubMed: 15515178]
24. Pennington BF, Moon J, Edgin J, Stedron J, Nadel L. The neuropsychology of Down syndrome: evidence for hippocampal dysfunction. Child Dev. Jan-Feb;2003 74:75. [PubMed: 12625437]

25. Reeves R, et al. A mouse model for Down Syndrome exhibits learning and behaviour deficits. Nature Genetics. 1995; 11:177. [PubMed: 7550346]
26. Siarey RJ, Coan EJ, Rapoport SI, Galdzicki Z. Responses to NMDA in cultured hippocampal neurons from trisomy 16 embryonic mice. Neurosci Lett. Sep 5.1997 232:131. [PubMed: 9310297]
27. Kleschevnikov AM, et al. Hippocampal long-term potentiation suppressed by increased inhibition in the Ts65Dn mouse, a genetic model of Down syndrome. J Neurosci. Sep 15.2004 24:8153. [PubMed: 15371516]
28. Hanson JE, Blank M, Valenzuela RA, Garner CC, Madison DV. The functional nature of synaptic circuitry is altered in area CA3 of the hippocampus in a mouse model of Down's syndrome. J Physiol. Feb 15.2007 579:53. [PubMed: 17158177]
29. Epp JR, Spritzer MD, Galea LA. Hippocampus-dependent learning promotes survival of new neurons in the dentate gyrus at a specific time during cell maturation. Neuroscience. Oct 26.2007 149:273. [PubMed: 17900815]
30. Gould E, Tanapat P, Rydel T, Hastings N. Regulation of hippocampal neurogenesis in adulthood. Biol Psychiatry. Oct 15.2000 48:715. [PubMed: 11063968]
31. Kim CH, et al. Lobule-specific membrane excitability of cerebellar Purkinje cells. J Physiol. Jan 15.2012 590:273. [PubMed: 22083600]
32. Usowicz MM, Garden CL. Increased excitability and altered action potential waveform in cerebellar granule neurons of the Ts65Dn mouse model of Down syndrome. Brain Res. May 22.2012
33. Burguiere E, et al. Spatial navigation impairment in mice lacking cerebellar LTD: a motor adaptation deficit? Nat Neurosci. Oct.2005 8:1292. [PubMed: 16136042]
34. Costa AC, Grybko MJ. Deficits in hippocampal CA1 LTP induced by TBS but not HFS in the Ts65Dn mouse: a model of Down syndrome. Neurosci Lett. Jul 15.2005 382:317. [PubMed: 15925111]
35. Hyde LA, Crnic LS, Pollock A, Bickford PC. Motor learning in Ts65Dn mice, a model for Down syndrome. Dev Psychobiol. Jan.2001 38:33. [PubMed: 11150059]
36. Fernandez F, et al. Pharmacotherapy for cognitive impairment in a mouse model of Down syndrome. Nat Neurosci. Feb 25.2007
37. Kleschevnikov AM, et al. Deficits in cognition and synaptic plasticity in a mouse model of Down syndrome ameliorated by GABAB receptor antagonists. J Neurosci. Jul 4.2012 32:9217. [PubMed: 22764230]
38. Petrosini L, Leggio MG, Molinari M. The cerebellum in the spatial problem solving: a co-star or a guest star? Prog Neurobiol. Oct.1998 56:191. [PubMed: 9760701]
39. Burguiere E, Arabo A, Jarlier F, De Zeeuw CI, Rondi-Reig L. Role of the cerebellar cortex in conditioned goal-directed behavior. J Neurosci. Oct 6.2010 30:13265. [PubMed: 20926652]
40. Feil R, et al. Impairment of LTD and cerebellar learning by Purkinje cell-specific ablation of cGMP-dependent protein kinase I. J Cell Biol. Oct 27.2003 163:295. [PubMed: 14568994]
41. Gao Z, van Beugen BJ, De Zeeuw CI. Distributed synergistic plasticity and cerebellar learning. Nat Rev Neurosci. Aug 1.2012 13:619. [PubMed: 22895474]
42. Schonewille M, et al. Reevaluating the role of LTD in cerebellar motor learning. Neuron. Apr 14.2011 70:43. [PubMed: 21482355]
43. Bambakidis NC, et al. Intravenous hedgehog agonist induces proliferation of neural and oligodendrocyte precursors in rodent spinal cord injury. Neurosurgery. Dec.2010 67:1709. [PubMed: 21107202]
44. van Reeuwijk J, Arts HH, Roepman R. Scrutinizing ciliopathies by unraveling ciliary interaction networks. Hum Mol Genet. Oct 15.2011 20:R149. [PubMed: 21862450]
45. Goodrich LV, Milenkovic L, Higgins KM, Scott MP. Altered neural cell fates and medulloblastoma in mouse patched mutants. Science. 1997; 277:1109. [PubMed: 9262482]
46. Weiss GJ, Korn RL. Metastatic basal cell carcinoma in the era of hedgehog signaling pathway inhibitors. Cancer. Nov 1.2012 118:5310. [PubMed: 22511370]

47. Currier, DG.; Polk, RC.; Reeves, RH. Progress in Brain Research. Dierssen, MaFRDLT., editor. Vol. 197. Elsevier; London: 2012. p. 223-36.

48. Mouton, PR. Principles and Practices of Unbiased Stereology: An Introduction for Bioscientists. The Johns Hopkins University Press; Baltimore: 2002. p. 214

49. Park S, et al. Elongation factor 2 and fragile X mental retardation protein control the dynamic translation of Arc/Arg3.1 essential for mGluR-LTD. Neuron. Jul 10.2008 59:70. [PubMed: 18614030]

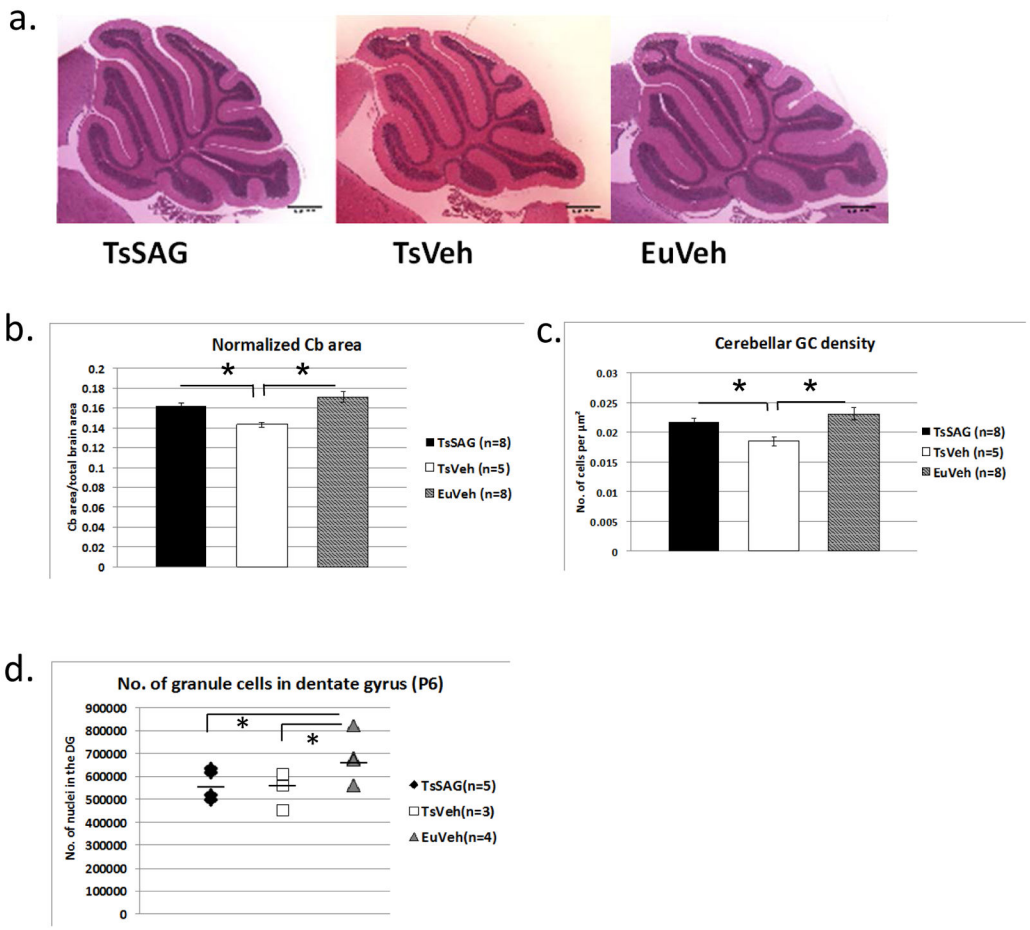

Fig. 1.

An injection of SAG at P0 normalizes cerebellar morphology in adult Ts65Dn mice. a) Representative sagittal images of TsSAG, TsVeh and EuVeh cerebella, ca. 4 months of age. H&E; scale bar is 1 mm. b) Cerebellar (Cb) cross-sectional area is restored to euploid levels in TsSAG mice. Both TsSAG and EuVeh are significantly larger than TsVeh. c) Cerebellar GC density is also restored in TsSAG mice. (b and c, MANOVA for normalized Cb area and GC density, Wilk's Lambda=0.278, F=0.583, Fisher's LSD test; TsSAG vs. TsVeh, p=0.02 and TsVeh vs. EuVeh, p=0.002). d) The number of granule cells in the dentate gyrus at P6 was determined using stereology and showed no significant effect of SAG treatment (means indicated by a bar, Fisher's LSD for pairwise comparisons, TsSAG vs. EuVeh p = 0.03 and for TsVeh vs. EuVeh, p = 0.02).

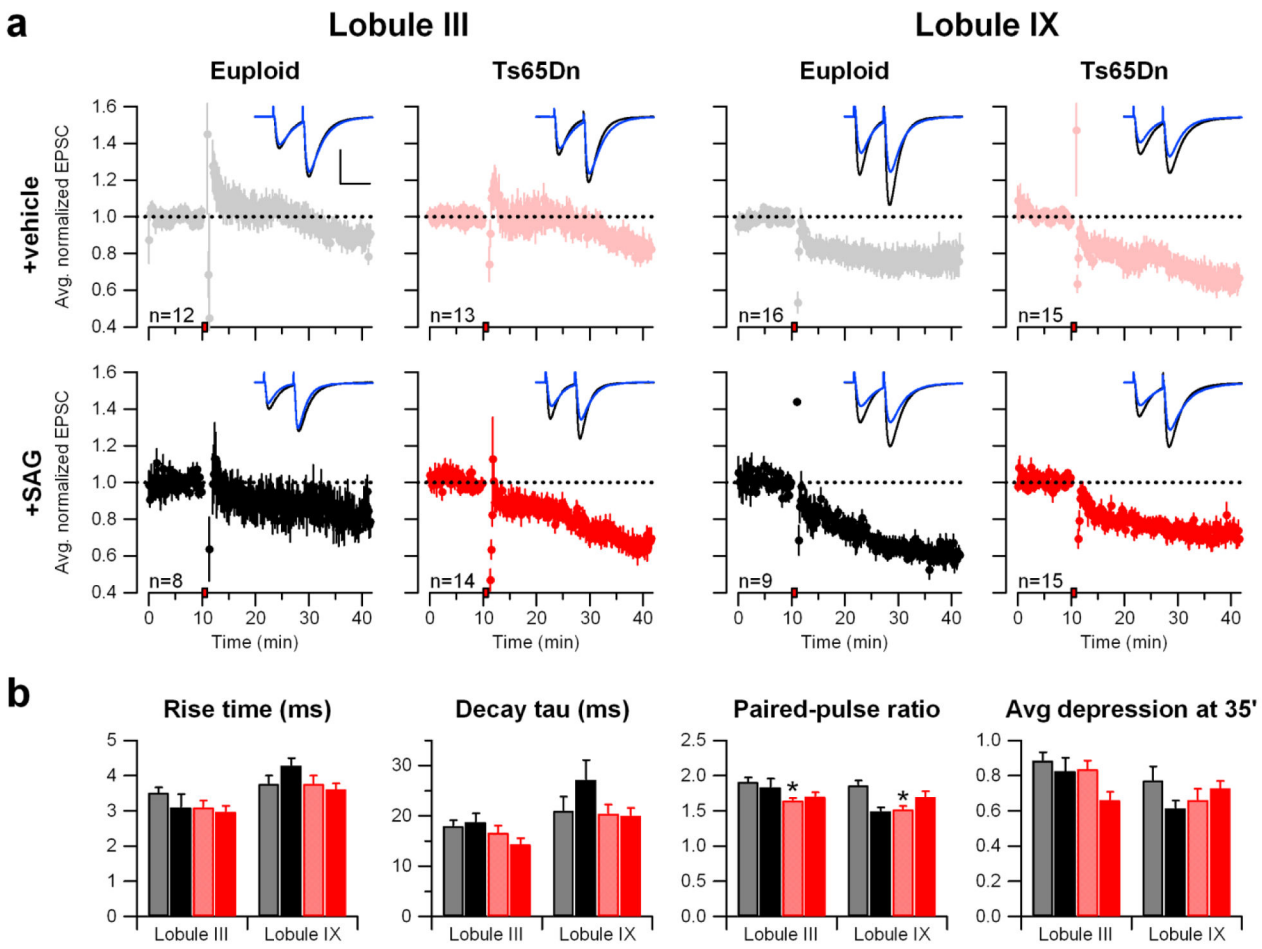

Fig. 2.

Cerebellar LTD is minimally different between Ts65Dn and euploid mice. a) Cerebellar long-term synaptic depression (LTD). EPSCs normalized to the baseline were averaged and plotted as a function of time for each group according to genotype (Euploid or Ts65Dn), treatment (vehicle or SAG), and cerebellar lobule (III or IX). The red box on the x-axis indicates the time of LTD induction. The error bars represent the SEM. The dashed line at 1.0 shows the position of the baseline. Representative traces before (black) and 25 minutes after (blue) LTD induction (t=35′) are shown superimposed. Scale bars = 50 msec, 200 pA. b) Bar graphs show the mean paired-pulse ratio measured at t=5′ (prior to LTD induction) and normalized EPSC at t=35′ (25′ after LTD induction). (Exact p-values for each measurement are in Table S2. On the figure, * p<0.05, **p<0.01, ***p<0.001).

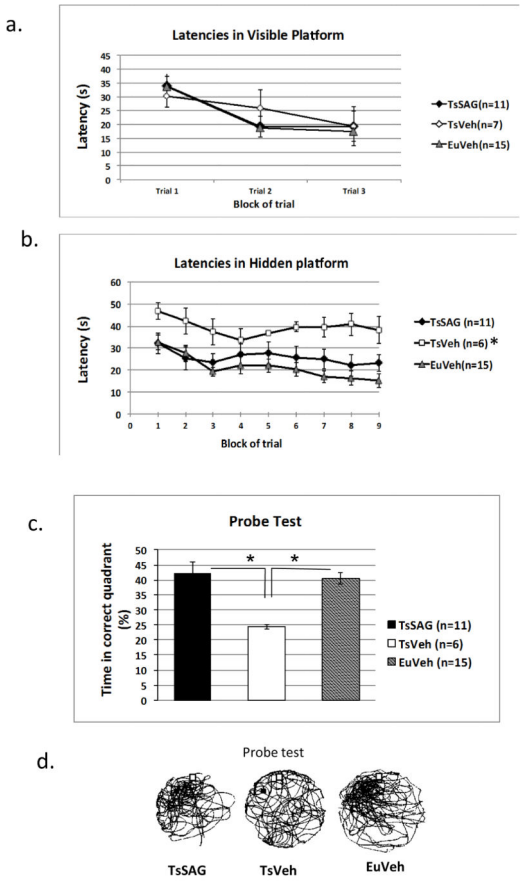

Fig. 3.

SAG corrects performance of trisomic mice in tasks dependent on hippocampus. a) TsVeh performed like EuVeh in MWM visible platform test, and there was no difference between TsVeh and TsSAG mice. Two way repeat measure ANOVA. b) Latencies in the MWM hidden platform test were significantly longer in TsVeh than in EuVeh or TsSAG (two way RM ANOVA, $F(2,29) = 6.5$, $p = 0.005$, alpha=0.05). Bonferroni-corrected p values showed a significant difference between TsVeh and both TsSAG p=0.003) and EuVeh (p=0.042), while TsSAG mice performed similarly to EuVeh (p= 0.91). c) In the probe test, EuVeh and TsSAG mice spent significantly more time in the correct quadrant than did TsVeh (Kruskal Wallis rank test, p = 0.001; Mann Whitney pair-wise comparison, TsVeh vs. TsSAG (p = 0.001) and TsVeh vs. EuVeh (p = 0.0001),. d) Representative search tracks in the probe test show that impaired search strategies used by TsVeh mice are corrected in TsSAG. Shown are representative tracks from a mouse of each group. The black box in the northwest quadrant is the former position of the platform.

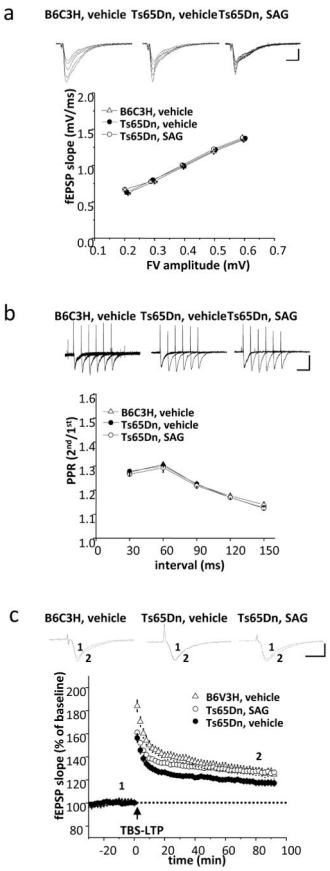

Fig. 4.

SAG rescues attenuated TBS-LTP in hippocampal slices from Ts65Dn mice. a) Relationship between fiber volley (FV) amplitude and fEPSP slope of the Schaffer collateral-CA1 synapses in slices from euploid and Ts65Dn mice (10- to 12-week-old males). Each point represents the mean ± SEM for a narrow range of fiber volley amplitudes and fEPSP slopes. (EuVeh slices, n=14; TsVeh slices, n=24; TsSAG slices, n=9). Scale bars: 1 mV, 10 ms. b) Representative traces in response to paired pulses in hippocampal slices derived from euploid and Ts65Dn mice (10- to 12-week-old males). Each plot point shows the mean ± SEM of the PPR (EuVeh slices, n=14; TsVeh slices, n=18; TsSAG slices, n=11). Baseline synaptic properties, including the fiber volley-fEPSP relationship and paired-pulse facilitation ratio (PPR) were normal in both TsVeh and TsSAG mice. Scale bars: 1 mV, 50 ms. c) SAG significantly enhanced TBS-LTP in slices from Ts65Dn mice. LTP was induced by theta burst stimulation (TBS: 5 bursts delivered at 5 Hz; each burst consisted of four stimuli at 100 Hz). TBS-induced LTP was significantly reduced in TsVeh (n=15) compared to either EuVeh (n=12) or TsSAG (n=19). (TsVeh vs. EuVeh slices, p=0.001 at t=30 min., p=0.038 at t=80 min.; TsVeh vs. TsSAG slices, p=0.006 at t=30 min., p=0.005 at t=80 min.; EuVeh vs. TsSAG slices, p=0.147 at 30min, p=0.97 at t=80min, compared to EuVeh slices by unpaired two-tailed Student's test). Scale bars: 1 mV, 50 ms.

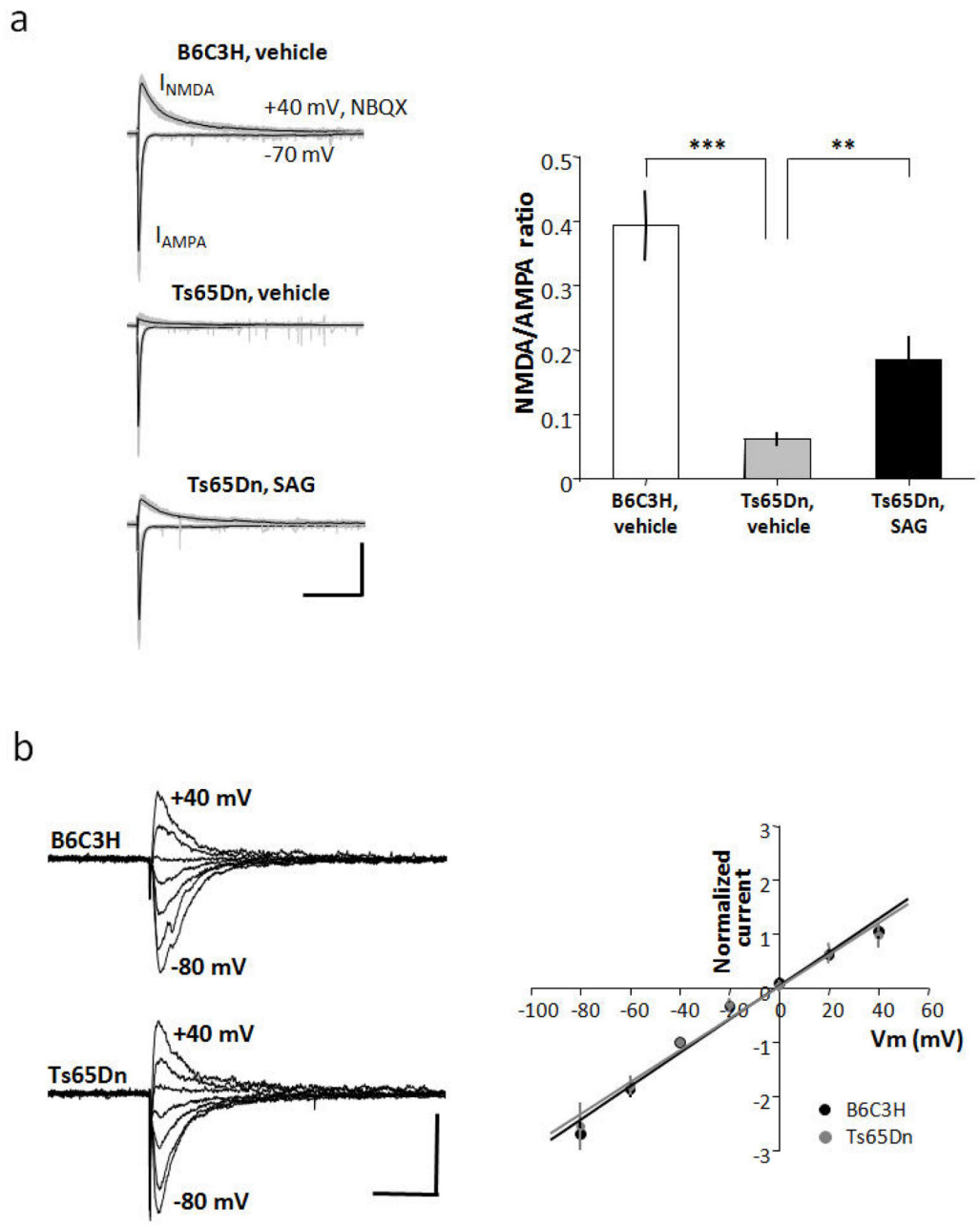

Fig. 5.

SAG partially rescues attenuated NMDA-EPSCs in hippocampal slices from Ts65Dn mice. a) Current-voltage (I–V) relationship in CA1 pyramidal neurons derived from euploid (n=4) and Ts65Dn (n=4) hippocampal slices (10- to 12-week-old male mice). Raw single traces show evoked excitatory post synaptic currents (EPSCs) obtained while holding postsynaptic cells at membrane potentials ranging from −80 mV to +40 mV in 20 mV steps recorded in the presence of D-AP5 (50 μM) and GABAzine (10 μM) to isolate AMPAR-mediated EPSCs. For measurement of I–V curves, spermine (100 μM) was added to block GluR2-lacking AMPARs at positive potentials. Graph shows I–V relationship normalized to the peak EPSC amplitude at −40 mV (Vm indicates membrane potential). The data were fitted by a line giving an estimate for the reversal potential of −0.9 mV (euploid in black) and −0.5 mV (Ts65Dn in gray), respectively (corrected for liquid junction potential). The voltage dependence of the evoked AMPA current was not significantly different between euploid and Ts65Dn. Scale bars: 100 pA, 50

ms. b) Raw (gray) and averaged (black) traces from a series of 20 consecutive evoked EPSCs recorded from hippocampal Schaffer collateral-CA1 synapses (10- to 12-week-old male mice). Peak AMPA currents were measured at −70 mV, and NMDA currents at +40 mV in the presence of NBQX. The NMDA/AMPA ratio was diminished in Ts65Dn neurons (n = 11) compared with euploid (n = 13). SAG treatment significantly increased NMDA currents in Ts65Dn neurons (n=11). Error bars represent the mean ± SEM. (TsVeh vs. TsSAG, p=0.003; EuVeh vs. TsVeh p=1.7E-5; EuVeh vs. TsSAG, p=0.006, unpaired two-tailed Student's t test). Scale bars: 200 pA, 250 ms.